Geophysical Journal International

Geophys. J. Int. (2023) **235,** 1325–1338
Advance Access publication 2023 July 31
GJI Gravity, Geodesy and Tides

https://doi.org/10.1093/gji/ggad306

Unraveling the contributions of atmospheric rivers on Antarctica crustal deformation and its spatiotemporal distribution during the past decade

Jingming Li [1,2] Wenhao Li,[1,3,4] C.K. Shum,[4,5] Fei Li,[6,7] Shengkai Zhang [6] and Jintao Lei[8]

[1] *State Key Laboratory of Geo-Information Engineering, Xi'an* 710054, *China. E-mail: wh_li@whu.edu.cn*
[2] *School of Civil Engineering, Southwest Forestry University, Yunnan* 650224, *China*
[3] *School of Geomatics Science and Technology, Nanjing Tech University, Nanjing* 211816, *China*
[4] *State Key Laboratory of Geodesy and Earth's Dynamics, Innovation Academy for Precision Measurement Science and Technology, Chinese Academy of Science, Wuhan* 430010, *China*
[5] *Division of Geodetic Science, School of Earth Science, Ohio State University, Columbus, OH* 43210, *USA*
[6] *Chinese Antarctic Center of Surveying and Mapping, Wuhan University, Wuhan* 430079, *China*
[7] *State Key Laboratory of Information Engineering in Surveying, Mapping and Remote Sensing, Wuhan University, Wuhan* 430079, *China*
[8] *School of Civil Engineering and Architecture, Guangxi University, Nanning* 530004, *China*

Accepted 2023 July 27. Received 2023 July 26; in original form 2023 March 21

SUMMARY

Atmospheric rivers (ARs) are efficient mechanisms for transporting atmospheric moisture from low latitudes to the Antarctic continent. AR events induce intense snowfall episodes, which increase crustal deformation. Here, we used an AR detection algorithm, via a spatial matrix operation to quantify the contribution of AR-induced snowfall in the Antarctic continent, 2010–2019. Our results reveal that the AR snowfall contribution to Antarctica primarily ranged from 9.28 to 29.73 per cent from 2010 to 2019, and there was an evident increasing trend from 2015 to 2019 (20.66 per cent in 2015 to 29.30 per cent in 2019). AR-induced snowfall is one of the factors influencing the surface deformation of the Antarctic continent, based on the hourly AR snowfall deformation calculations for the Antarctic continent, both the average and maximum crustal deformation or displacement tends to be greatest near the coastline, while the displacement is less affected by AR further inland.

Key words: Global change from geodesy; Satellite geodesy; Antarctica.

1 INTRODUCTION

The Antarctic continent, like many deserts, receives a large portion of its annual precipitation from a few heavy precipitation events. Studies have shown that extreme precipitation in the first 10 per cent of the Antarctic ice sheet can contribute 40–60 per cent of total interannual precipitation (Turner *et al.* 2019). Atmospheric rivers (ARs), one of the most typical and dramatically influential climate extremes, have a very important impact on Antarctic snowfall and melting processes. Defined by the American Meteorological Society (AMS GM) as a long, narrow (average length of 1600 km, width of 640 km), short-lived, intense horizontal water vapour transport corridor, usually associated with low-level rapids preceding a cold front of a temperate cyclone (Zhu & Newell 1994; Neiman *et al.* 2008; 2013, Ralph *et al.* 2017; Nash *et al.* 2018). In recent years, most near-coastal Antarctic regions have experienced multiple AR extremes on rare annual occurrences, and notably exhibit a year-to-year increase (8 in 2010 to 16 in 2019), resulting in significant impacts on the ice sheet mass balance. AR login in polar regions can induce extreme weather such as heavy rain, snowstorms and extremely cold weather (Gimeno *et al.* 2021), has a significant contribution to polar climate and environmental change, and also influences the global climate cycle (Wille *et al.* 2021).

The increasing frequency of AR occurrences since 1979 has led to increased precipitation (mainly snowfall) on the Antarctic ice sheet, and gradually increased share of relative contributions. In particular, AR transports of water vapour and air to the poles and enhances the intensity of Antarctic climate variabilities (Shields & Kiehl 2016; Pohl *et al.* 2021). It has been shown that AR is the primary cause of many of the interannual maximum (AM) precipitations in Western Europe, the Western United States and other parts of the world that play a critical role in triggering heavy precipitation and acting as a water supply (Lavers & Villarini 2013; Ralph *et al.* 2017). In addition, AR can trigger mixed rainfall and snowfall events in some areas (Viceto *et al.* 2022). Although ARs are relatively rare over the Antarctic coastal region, they have a significant impact on precipitation climatology, with AR accounting for at least 10–20 per cent of total cumulative snowfall in East Antarctica and also associated with most extreme precipitation events. In the investigation of a heavy snowfall event associated with AR, located

in the East Antarctic coastal region, the event accounted for 24 per cent of the annual snowfall (Terpstra *et al.* 2021; Wille *et al.* 2021). In addition to its impact on climate, AR also influences the melting or the accelerated mass loss of ice sheet mass in the Antarctic and Greenland, and AR constitutes a major driver of surface melting in Antarctica (Francis *et al.* 2020; Mattingly *et al.* 2020; Djoumna & Holland 2021; Djoumna *et al.* 2021). High-intensity AR can weaken the stability of the Antarctic Peninsula ice shelf (Wille *et al.* 2022). It is well known that the drivers of surface melt in West Antarctica are critical to understanding future ice loss and global sea level rise, and are closely related to surface melt in Antarctica (Scott *et al.* 2019; Wille *et al.* 2019). AR contributes to the surface mass balance (SMB) of the Antarctic ice sheet by causing large snowfall events in East Antarctica. High snowfall events in West Antarctica are a key influence on its mass balance and can mitigate sea level rise due to global warming, and the occurrence of AR events is critical for predicting future sea level rise (Gorodetskaya *et al.* 2014; Payne *et al.* 2020; Maclennan & Lenaerts 2021; Adusumilli *et al.* 2021; Maclennan *et al.* 2021). AR-induced intense precipitation causes crustal deformation and surface height changes in Antarctica, with some studies suggesting a general increase in snow surface height in West Antarctica in 2019, with 63 per cent of these events associated with AR (Adusumilli *et al.* 2021). Studies of crustal deformation and ice cover loss in West Antarctica have shown plausible erroneous estimated crustal deformation in Antarctica, particularly underestimated crustal uplift rates in some areas, and that discrepancies exist that cannot be explained simply by the elastic response to ice loss (Bevis *et al.* 2009). AR has varying degrees of impact along the Antarctic continent's coastline and extends into the continental interior (Shields *et al.* 2022).

Prior published studies have focused on AR detection, analysis of climate influences, polar SMB and ice shelf stability (Gorodetskaya *et al.* 2014; Wille *et al.* 2019, 2021; Maclennan & Lenaerts 2021; Collow *et al.* 2022; Maclennan *et al.* 2022; Lenaerts *et al.* 2019). There is a paucity of studies that accurately quantify and assess the impact of heavy snowfall due to AR. Further, since Antarctic mass balance is sensitive to short-term extreme meteorological events, and the resulting transient and abrupt signals of crustal deformation are revealed by GNSS observed coordinate time-series (Wille *et al.* 2019; Payne *et al.* 2020; Maclennan *et al.* 2022). Therefore, further studies are needed to determine the time of AR appearance, the spatial extent of login, the pattern of AR activity and the contribution of AR to snowfall. Including the correlation between login duration, coverage, frequency and contribution, the impact of AR-induced snowfall on Antarctica surface deformation or displacement, especially for the abrupt transient signal of the crust caused by strong AR snowfall episodes is not well quantified. Here, a method to quantify the contribution of AR-induced snowfall on the Antarctic continent is the focus of this work, and the year-by-year AR contribution from 2010 to 2019 is calculated and analysed. We extract the AR snowfall over the Antarctic continent and use a load-deformation model to further analyse the influence of AR snowfall-induced Antarctic surface deformation.

2 DATA AND METHOD

2.1 Data

In this study, we used MERRA-2 IWV (Integrated Water Vapour), vIVT data distributed by the Atmospheric River Tracking Method Intercomparison Project (ARTMIP) to extract AR. The study time period is from 2010 January 01 through 2019 December 31. IWV and vIVT data are mainly used to extract the spatial and temporal extent of AR. We then used MERRA-2 based on snowfall data for the corresponding period (2010–2019), which was obtained from the National Aeronautics and Space Association (NASA). In particular, the AR data temporal resolution of 1-hr, the temporal resolution of the snowfall data is also 1-hr and the spatial resolution of 0.5° × 0.625°, the spatial span of the study area is 60°S–85°S, 180°W–180°E, over the Antarctic continent. When calculating the snowfall displacement, the Antarctic GNSS stations need to be set up in the program, and information about the longitude and latitude locations of the stations on the Antarctic continent can be obtained from the UNAVCO data centre. The results of the AR snowfall load deformation calculations are validated using continuous GNSS time-series with a temporal resolution of 5 min, which can be obtained from the Nevada Geodetic Laboratory.

2.2 AR detection algorithm

ARs transport water vapour from low to high latitudes in the shape of narrow filamentary channels, and ARs produce intense rainfall and snowfall events. To investigate and quantify the contribution of AR to snowfall in Antarctic continental gauges, this paper composes and analyses methods to detect AR, focusing on integrated water vapour (IWV) and integrated water vapour transport (IVT). In this study, the AR detection algorithm of Wille *et al.* (2021, updated consideration of the v-component of the meridional wind speed, vIVT) is further updated with the latitude of AR detection in the Antarctic continental study area of this paper, updating the latitude span from the original 37.5°–80° S to 60°–85° S, the purpose is to weaken the moisture transport data from the subtropics and mid-latitudes that interfere with this study. On this updated range, an AR is recorded if the algorithm detects a continuous filamentary channel extending at least 20° in the meridional direction for each detected vIVT. IWV (kg m^{-2}), IVT (kg m^{-1} s^{-1}) and vIVT (kg m^{-1} s^{-1}) can be described by eqs (1), (2) and (3), respectively. Eq. (1) is mainly inquiring how to detect AR using water vapour data, and eq. (2) is mainly studying the detection of AR in the Antarctic region, however, eq. (3) is the specific detection of AR for the study area of the Antarctic continent after reclassifying the meridional wind speed, and eq. (3) which is more suitable for the Antarctic continent is used in the detection of AR in this paper.

$$\mathrm{IWV} = -\frac{1}{g}\int_{\text{surface}}^{\text{top}} q\,dp \tag{1}$$

$$\mathrm{IVT} = -\frac{1}{g}\int_{\text{surface}}^{\text{top}} qV\,dp \tag{2}$$

$$\mathrm{vIVT} = -\frac{1}{g}\int_{\text{surface}}^{\text{top}} qv_m\,dp \tag{3}$$

IWV, IVT and vIVT are mainly calculated spatially based on the humidity ratio. Eqs (1), (2) and (3) in which q(kg kg^{-1}) is the humidity ratio, g(m s^{-2}) is the gravitational acceleration, p(hPa) is the atmospheric pressure and V(m s^{-1}) is the wind speed in eq. (2), however, eq. (3) is an improvement of eq. (2) where the v_m(m s^{-1}) component is the further considered meridional wind speed and denotes the updated AR detection by vIVT.

2.3 Simplified calculation of AR snowfall spatial matrix

Quantitative calculations are a very important task in data processing and research of AR and snowfall. However, it poses a challenge

due to the need to consider temporal ranges, spatial coverage and spatiotemporal resolution. Here, we convert the snowfall calculation and extracted AR snowfall into a matrix of operations in this paper, which has the advantage of faster and more accurate data processing. Therefore, first, a one-to-one correspondence of spatial locations is needed to ensure that the data and variables (e.g. snowfall) are matched with each other in the actual spatial locations and in the spatial matrix. Secondly, the spatial resolution needs to be considered. Finally, the spatial bits of the matrix are calculated to realize the operation of the research data in the corresponding spatial position. This processing can accurately and quickly handle the research data (such as merging calculation, segmentation calculation, extraction calculation, superposition calculation, normalization calculation, etc.) and simplify the calculation work. For the extraction problem of AR snowfall, the submodule of AR latitude and longitude to matrix bits can be established, and finally, the constant superposition calculation of year-by-year total snowfall and AR recorded snowfall spatial matrix can be performed, respectively, to realize the extraction of annual snowfall and AR snowfall.

AR snowfall refers to the snowfall triggered at the time of AR events, and it is found by calculation that this part of snowfall contributes more to the overall snowfall. The idea of quantitative calculation of AR snowfall is divided into three steps. First, the AR event is detected to obtain all the time nodes and duration of AR time occurrence, and also the spatial extent covered by AR needs to be extracted, and this work will provide support to determine the snowfall caused by AR. Second, a spatial matrix (corresponding to the actual latitude and longitude) is created for placing snowfall based on the spatial resolution of the snowfall data. Third, the snowfall data at a certain temporal resolution (e.g. by 1 or 3 hr) are merged, and the temporal ranges of the merge can be reasonably assigned according to the research objectives, and then the snowfall corresponding to the AR events are placed into the created spatial matrix. The snowfall due to AR can be easily obtained through matrix operations, the snowfall data can be further visualized, and the spatial distribution of snowfall due to AR can also be obtained.

Since the spatial resolution of snowfall data used in this study is $0.5^\circ \times 0.625^\circ$, a snowfall spatial matrix of 61×576 is created for the spatial resolution of snowfall data. In addition, the spatial extent of snowfall where the AR is located is converted using the latitude and longitude to matrix bit submodule program to obtain the matrix spatial location where the AR snowfall is located, and finally, the spatial matrix is used to perform operations on the AR snowfall and interannual snowfall. The spatial matrix is shown in eq. (4), the main equation of the longitude–spatial matrix column position is shown in eq. (5), and the main equation of the latitude–spatial matrix row position is shown in eq. (6) used in the program transformation module.

$$\begin{bmatrix} 1 & \dots & 1*n \\ \vdots & \ddots & \vdots \\ m & \dots & m*n \end{bmatrix} \tag{4}$$

$$\mathrm{col} = \left(\frac{L+180}{u}\right) + 1 \tag{5}$$

$$\mathrm{row} = \left(\frac{W+90}{k}\right) + 1 \tag{6}$$

In this study, $m = 61$ and $n = 576$ in eq. (5), L is the longitude boundary of the extracted AR, u is the spatial resolution, where $u = 0.625$, and col is the column of the matrix after conversion; W is the latitude boundary of the extracted AR, k is the spatial resolution, where $k = 0.5$, and row is the row of the matrix after conversion in eq. (6).

The total interannual snowfall needs to be determined first, and then the AR snowfall needs to be calculated to derive the ratio of AR snowfall to total snowfall. Regarding the calculation of interannual snowfall, the spatial matrix calculation can be used, while the AR snowfall calculation is based on the spatial matrix calculation by first converting the AR spatial position using the program submodule mentioned. After the AR spatial position is converted to the spatial matrix bit, the AR snowfall can be obtained by using the spatial matrix superposition calculation, and the snowfall contribution expression is shown in eq. (7).

$$P = \frac{\mathrm{ArS}}{\mathrm{TotArS}} \tag{7}$$

In eq. (7), P is the AR snowfall contribution, ArS is the AR snowfall and TotArS is the total interannual snowfall. The interannual total snowfall and AR snowfall are calculated in this way and the contribution is calculated for 2010–2019.

The main purpose of the normalized matrix operation is to get the AR-logged snowfall frequency, and then the visualization process can visually obtain the high-, medium- and low-frequency areas where AR logs in the Antarctic continent. If we only deal with the AR snowfall matrix a problem arises, for the different values in each AR snowfall matrix, if we do a direct matrix superposition calculation we cannot clearly separate and accumulate them to the corresponding spatial locations. Therefore, by normalizing the AR snowfall data to get the normalized matrix of each AR. At this moment, each matrix has the value of the location all 1, and indicates that the AR snowfall frequency was recorded once, no AR snowfall frequency of the location is 0. Then all the matrices from 2010 to 2019 are superimposed (e.g. the same location is tested and calculated 3 times, and only 2 AR snowfall frequencies occurred, then the value of this matrix location superimposed calculation is 2, indicating that the location AR snowfall frequency is 2). If there are multiple snowfalls at the same location, the corresponding matrix for location 1 is accumulated multiple times, and the final value in the matrix is the frequency of AR, and the data obtained can be analysed to find out the high-frequency areas where AR occurs. The calculation results are shown in Fig. 1 below.

The normalized superposition of AR snowfall is shown in Fig. 1(a) shows the normalized superposition of AR snowfall, and (b) shows the visualized distribution of AR occurrence frequency in the Antarctic continent after superposition. The row and column axes in Fig. 1(a) indicate the row and column positions of the spatial matrix corresponding to AR snowfall, and the AR layer axes indicate the weights of the matrix superposition calculation, corresponding to the AR snowfall quantities in the spatial position superposition calculation. The 0 and 1 in each layer indicate the normalized value of AR snowfall quantity, and 1 indicates that one AR is recorded at that spatial location. when multiple AR snowfall events occur at the same spatial location, 1 will be accumulated multiple times at that spatial location, and finally the corresponding AR snowfall frequency at each spatial location is obtained. Fig. 1(b) represents the recording frequency orthogonal map of the Antarctic continent used to visualize the AR snowfall frequency, and from the example map given, it can be seen that the AR snowfall frequency map can be used to understand in which areas the AR snowfall is mainly concentrated.

Fig. 1(b) represents the logged frequency orthomosaic of the Antarctic continent for visualizing the AR snowfall frequency, and from the example map given, it can be seen that the AR snowfall

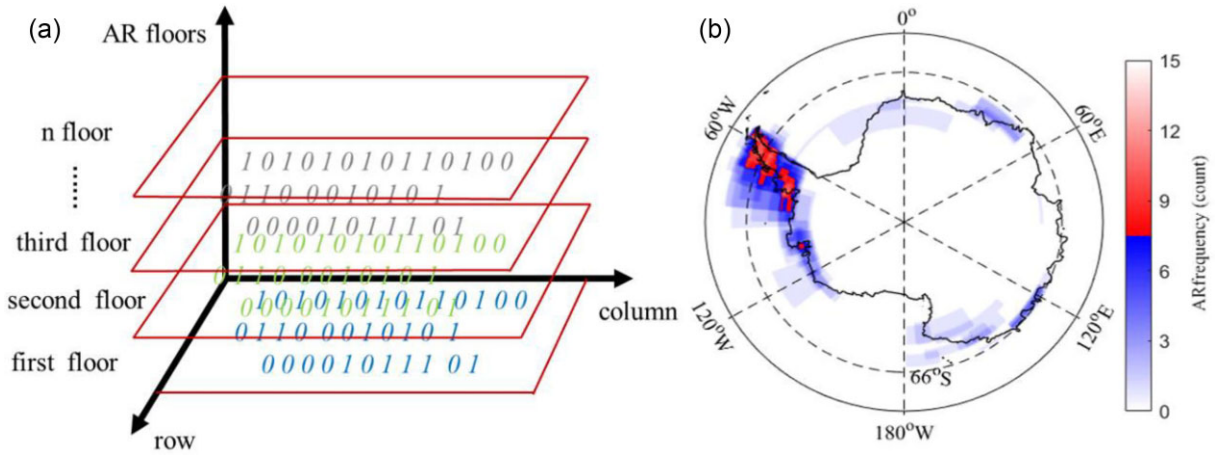

Figure 1. AR snowfall normalized superposition

frequency map can be used to understand the areas where the AR snowfall is mainly concentrated.

2.4 Calculation of load-deformation displacement

Calculation of Antarctic continent snowfall displacement using a load-deformation model (Martens *et al.* 2019). First, we need to configure the program computing environment, import the required load-deformation model and data format conversion module, displacement calculation module and significant GPS station displacement impact estimation module (with a radius of 200 km circle), and debug and appropriately modify the programs of all modules to achieve the calculation of snowfall displacement on the Antarctic continent that can be realized in this study. The modification part mainly involves the adjustment of the specific time resolution detection, temporal ranges, spatial resolution, and latitude and longitude position of the Antarctic GPS station applicable to this study. Finally, an estimate of the displacement produced by AR snowfall on the Antarctic continent is obtained and calculated precisely to the eastward, northward and vertical displacements.

To control the impact of AR events on snowfall in the Antarctic continent from a macroscopic perspective. In this study, the following experimental design and work were done, first, all the snowfall data from 2010 to 2019 were data merged to encapsulate 10 yr of data into one complete data arranged by time-series, and then projected 10 d before and after each time node of AR event login and leaving for calculation, increasing the time range of AR occurrence can attenuate the AR time. The inaccurate identification of nodes, the delay in the appearance of some ARs and the impact of extreme weather on ARs.

To convert the AR-induced snowfall to the displacement generated by the Antarctic continent, this study constructs a computational model for snowfall displacement in the Antarctic continent based on the load-deformation computational model. As mentioned in Martens' original intention of constructing the Earth load deformation load model, the Earth, and other celestial bodies are constantly influenced by some material and surface forces, such as gravity and the mass loading of some substances on the Earth's surface. While the forces are occurring, the mutual forces on the surface matter and the Earth's surface in contact produce a corresponding deformation, on the one hand, of the matter and on the other hand, the Earth's surface undergoes deformation. The degree of surface deformation may depend on the distribution of material properties, internal mass and elastic modulus of the material in contact. Therefore, in their study, a mass load-deformation model is developed to calculate the deformation of the Earth by material action with time, which can simulate the surface deformation on the one hand and help us to analyse the causes of deformation and perform some inversion studies on the other hand.

This paper precisely uses the idea of the mass loading-deformation model for deformation displacement calculation, and what we study is exactly about the deformation generated by AR snowfall in the Antarctic continent, they are the northward, eastward and vertical displacements. Our study hopes to provide some favourable references to the environmental changes in Antarctica. In particular, they are mainly AR in Antarctic climate (snowfall) characteristics and caused by surface deformation characteristics.

3 RESULT

3.1 AR spatiotemporal ranges

Extraction of AR events. The purpose is to extract the hour-by-hour occurrences of ARs in that temporal range and the spatiotemporal ranges of each AR occurrence are recorded. The spatial ranges are shown in Fig. 2 below (2010–2019), and the number of ARs appearing year-by-year, and hours are shown in Fig. 3.

Figs 2(a)–(j) denote the spatiotemporal ranges corresponding to the ARs extracted from 2010 to 2019, respectively, with different colours indicating the subdivisions of the corresponding AR logins. AR logins in the Antarctic Peninsula were observed every year, most notably in 2010, 2013, 2016, 2017, 2018 and 2019, with frequent AR logins in only two of the years 2010–2015 (2010 and 2013) and extensive AR logins in the Antarctic Peninsula every year between 2016 and 2019. Second, ARs logged frequently in the Amundsen region in 2010, 2013, 2015, 2016 and 2019, with 2013, 2015 and 2019 being the most pronounced. AR logins in the Southeast Antarctic were mainly concentrated in 2010, 2011, 2015, 2018 and 2019.

Fig. 3 shows the number (left vertical axis) and duration (right vertical axis) of AR login. Generally, AR entering and leaving the Antarctic continent is a continuous process, but there are a few cases of sudden jumps into the Antarctic continent and instant disappearance. In this paper, we take this factor into account and consider the

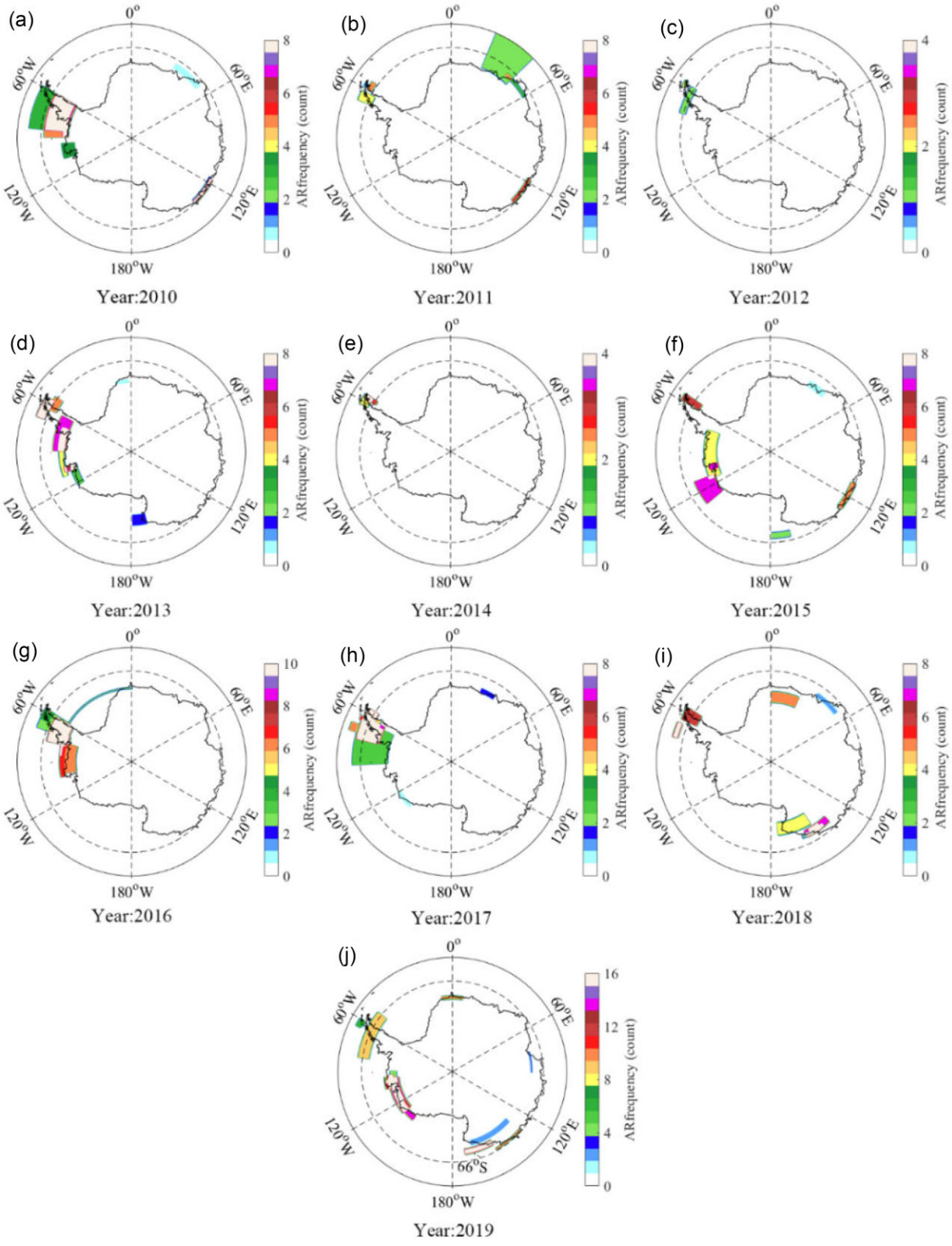

Figure 2. AR spatiotemporal range.

uncertainty in AR detection. At the same time, we want to control this uncertainty to avoid the impact on the overall detection accuracy caused by too large, and the uncertainty is increased by about 10 per cent in the current login duration and range when recording AR. The results of calculating the length and number of AR logins for 10 yr showed that the number of AR logins ranged from 7 to 16 for the years 2010–2019, except for 2012 and 2014 when the number of AR logins was low, and the length of logins ranged from

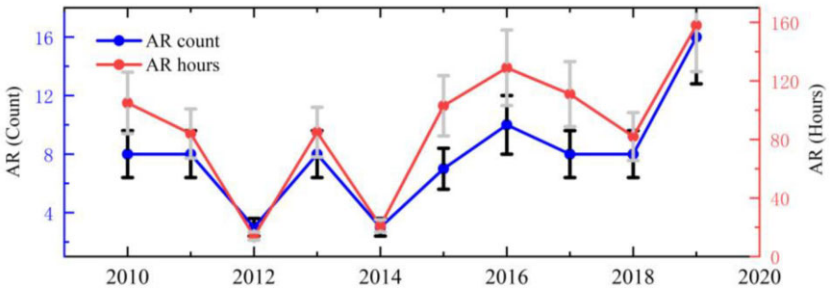

Figure 3. Number and length of AR logins.

14 to 158 hr. The results show that the accumulation of the number of logins leads to longer logins.

3.2 AR snowfall load-deformation displacement results

Before calculating the total AR snowfall displacement for 2010–2019, the snowfall displacement for one year (2010) was first studied. A uniform conversion to the netCDF data file format of the load-deformation model is required prior to the calculation, and then the snowfall data are read in as a time-series and at a specified temporal resolution using the read data subfunction. The location of the Antarctic GPS station also needs to be imported, and the calculation is performed with the station (here, the CAS1 station of the IGS organization) as the reference base, and finally, the displacement is calculated in the model, and the results are shown in Fig. 4 below.

Fig. 4(a) shows the eastward snowfall displacement, (b) shows the northward snowfall displacement and (c) shows the vertical snowfall displacement. From Fig. 4, it can be seen that the snowfall displacement fluctuates very little in the plane and more in the vertical direction. If the AR influence is taken into account in the snowfall displacement, combined with the month of AR occurrence in 2010 extracted in Section 3.1 and marked in Fig. 4(c) using coloured rectangles, the peak of displacement fluctuation in the figure and the position marked by coloured rectangles overlap more, according to which it can be tentatively presumed that the AR event occurring in the Antarctic continent has some influence on the occurrence of displacement. The existence of this pattern cannot be fully determined from this small experiment, so the AR events occurring in the total temporal ranges are studied as a whole and are treated.

Before calculating the snowfall displacement, the position information of the GPS station in Antarctica needs to be imported as a reference for the displacement calculation. Taking the displacement significant impact range (200 km) of the IGS organization and POLENET organization as a reference, a total of 34 GPS stations such as CAS1 station, DAV1 station and BEAN on the Antarctic continent were selected. Finally, the snowfall displacements were processed and calculated for the AR events with an extended time range, and the results are shown in Table 1 below.

The calculation results in Table 1 show that the maximum displacement due to AR snowfall is 0.83 mm for Ronne Ice Shelf, 1.34 mm for NAP, 0.95 mm for Ross Ice Shelf, 1.63 mm for the Amundsen Sea, 1.56 mm for East Antarctica and 1.56 mm for SAP.

In addition, new Levels have been added to characterize the displacement at different locations along the Antarctic continental coastline and to visualize it in combination with the distribution map of GPS stations on the Antarctic continent, as shown in Fig. 5.

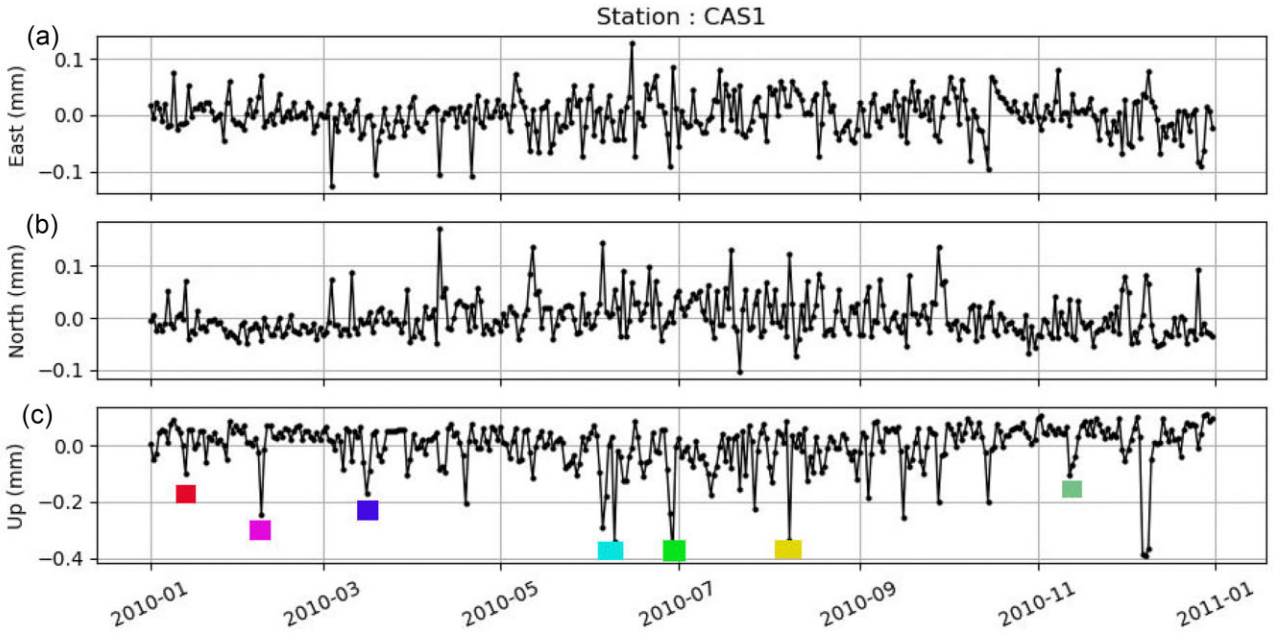

Figure 4. Displacement of CAS1 measurement station in 2010.

Table 1. Displacement of GPS stations by hourly (mm).

Location	GPS-sta	Max -disp	Avg -disp	Dist (km)	Level	Location	GPS-sta	Max -disp	Avg -disp	Dist (km)	Level
Ronne Ice Shelf	HOWN	0.83	0.08	432.98	3	Ross Ice Shelf	DAV1	0.90	0.08	9.17	1
	HAAG	0.83	0.09	375.69	2		FIEO	0.95	0.06	95.05	2
	MCM4	0.62	0.05	631.88	4		FLM5	0.45	0.05	78.06	3
	BEAN	0.82	0.08	250.01	1		FTP4	0.63	0.05	104.10	4
NAP	DUPT	1.19	0.15	0.69	e	Amundsen Sea	BERP	1.63	0.13	36.00	a
	FONP	1.22	0.13	1.26	f		INMN	1.36	0.11	69.25	c
	HUGO	1.10	0.13	512.22	h		LPLY	1.60	0.14	42.34	b
	OHI2	1.24	0.12	0.68	c		THUR	1.22	0.13	69.52	d
	OHI3	1.24	0.12	0.68	c		LTHW	1.00	0.11	136.37	e
	CAPF	1.28	0.11	0.33	a		KHLR	0.90	0.10	252.06	f
	PALM	1.28	0.15	0.52	b	East Antarctica	CAS1	1.56	0.10	3.78	3
	PALV	1.28	0.15	0.52	b		DUM1	1.43	0.13	0.55	1
	ROTH	1.20	0.14	0.55	d		MAW1	1.50	0.09	0.71	2
	SPGT	1.21	0.14	1.20	e		VESL	1.26	0.09	138.66	5
	VNAD	1.34	0.15	6.40	g		SYOG	1.34	0.10	4.89	4
						SAP	JNSN	1.56	0.12	179.22	c
							SUGG	1.10	0.09	239.44	d
							WLCH	1.03	0.11	115.65	b
							TRVE	1.28	0.13	34.03	a

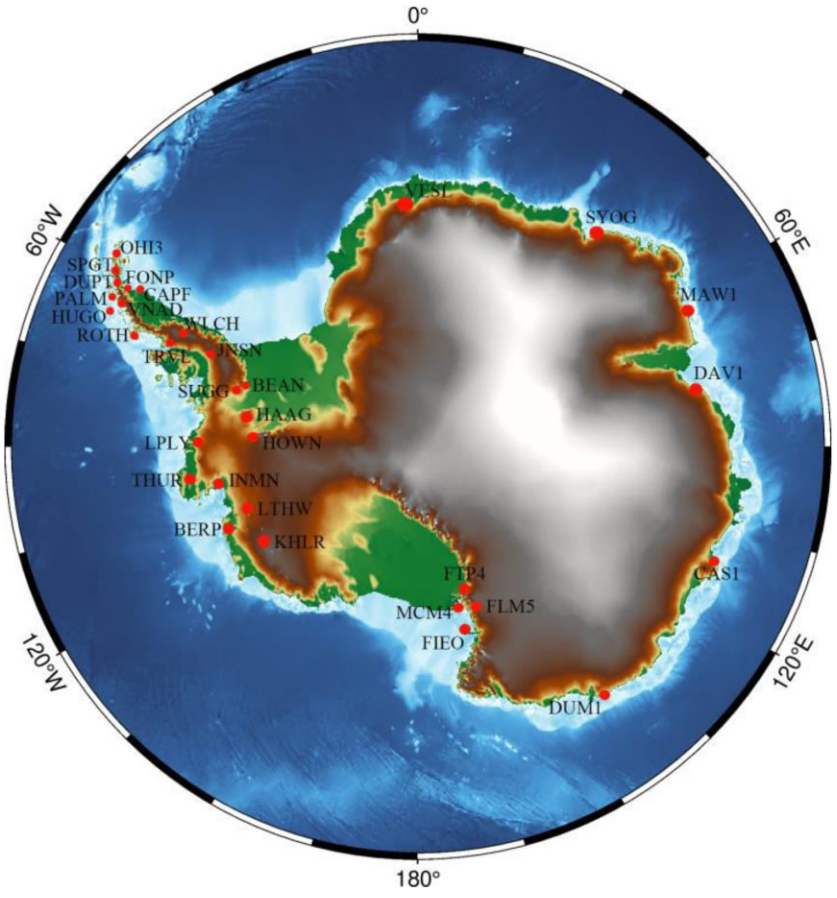

Figure 5. GPS site distribution.

Numbers and letters are used in Levels to distinguish the intensity of the impact to facilitate the division of stations into regions in the table; the smaller the number or the closer the letter is to a, the closer it is to the coastline (at the same time, we have added the distribution map of GPS stations in the Antarctic continent and the distance values from the stations to the coastline as reference). To determine the effect of distance from the coastline on the displacement, the analysis was carried out simultaneously from the maximum displacement

and the average displacement. The results show that generally the closer to the coastline, the greater the effect on displacement. For example, in Ronne Ice Shelf, the BEAN station is closest to the coastline and MCM4 is farthest from the coastline, with a maximum displacement of 0.82 mm (BEAN)–0.62 mm (MCM4) and an average displacement of 0.08 mm (BEAN)–0.05 mm (MCM4). Another example is that in East Antarctica, the CAS1 station is the closest to the coastline and VESL is the farthest from the coastline, with a maximum displacement of 1.56 mm (CAS1)–1.26 mm (VESL) and an average displacement of 0.10 mm (CAS1)–0.09 mm (VESL).

3.3 Snowfall data visualization and analysis

To accurately integrate snowfall data as well as AR frequency data with the Antarctic continent, this paper visualizes and analyses them (Pawlowicz 2020). Here, we analyse the frequent login areas, login coverage of AR in the Antarctic continent, as well as AR snowfall and total snowfall in the Antarctic continent from the annual visualization data for 2010, 2011 and 2015, as shown in Fig. 6 below.

Figs 6(a)–(c) correspond to the annual snowfall, AR snowfall and AR login frequency in 2010, (d)–(f) correspond to the annual snowfall, AR snowfall and AR login frequency in 2011 and (g)–(i) correspond to the annual snowfall, AR snowfall and AR login frequency in 2015. The red discs correspond to the Antarctic Peninsula, the green discs to Marie Byrd Land, the yellow discs to Adélie Land and Wilkes Land and the light blue discs to Enderby Land.

Without considering the effect of AR on snowfall, the annual snowfall in Figs 6 (a), (d) and (g), show that the snowfall in the two regions between Adélie Land and Wilkes Land and the Antarctic Peninsula, which are located in the Antarctic continent, is significantly higher than the other plates by colour shades.

When considering the effect of AR on snowfall, the spatial extent of AR is calculated by pre-calculating the snowfall where AR is located as shown in Figs 6(b), (e) and (h), the areas with more significant snowfall coincide with those roughly estimated, and other areas with more significant snowfall that cannot be identified by the naked eye are located. Combined with the AR contribution to Antarctic continent snowfall calculated, the AR contribution to Antarctic continent snowfall calculated for 2010–2019, excluding the very small and very large disturbances, is typically in the range of 9.28–29.73 per cent, which shows consistency with the roughly

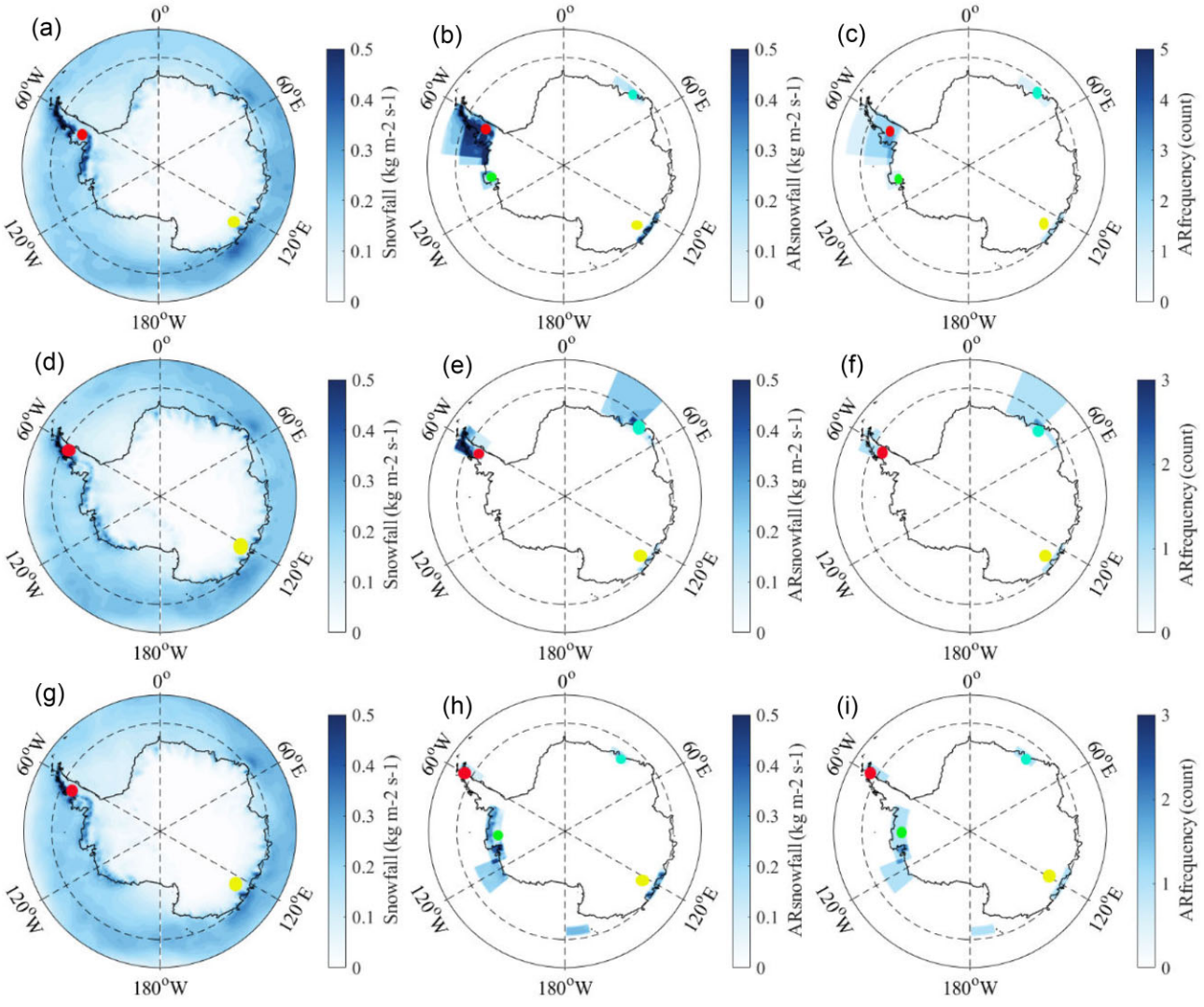

Figure 6. Annual snowfall (left-ahnd column), AR snowfall (middle column) and AR frequency (right-hand column).

estimated AR contribution to Antarctic continent snowfall of 10–20 per cent (Gorodetskaya *et al.* 2014; Wille *et al.* 2021).

In addition, the spatial range of AR occurrences presented in Fig. 2 was then analysed in conjunction with the hours calculated in Fig. 3. In the previous research work, the exact duration of each AR occurrence was extracted and calculated, and the total annual AR login duration was counted by year, with the exact duration ranging from 14 to 158 hr. It can be visualized from Figs 6(b), (e) and (h) that the spatial extent logged by AR is only a very small fraction. Therefore, the combination of the short duration and small spatial extent of the AR in the Antarctic continent can be inferred that the impact of AR on snowfall in the Antarctic continent is very informative.

In Section 3.1, snowfall calculations were performed year-by-year for the years 2010–2019, then this will be studied and analysed for the total temporal ranges of this study. The total snowfall, AR snowfall and AR snowfall frequency from 2010 to 2019 are shown in Fig. 7 below.

The snowfall caused by AR in Antarctica is mainly distributed in Antarctic Peninsula and Marie Byrd Land in West Antarctica, and Adélie Land, Wilkes Land, and Enderby Land in East Antarctica from (b) or (c) in Fig. 7. The Antarctic Peninsula in West Antarctica is the most influential, and the northward extension of the Antarctic Peninsula in West Antarctica is the most influenced by AR as can be visualized in Figs 7(b) and (c). This feature can be used to make a general control of the impact of AR on snowfall in Antarctica and provide a reference for future AR impact characteristics or subsequent research on AR and snowfall in Antarctica.

Finally, a brief summary and analysis of the preliminary work of AR affecting the snowfall in the Antarctic continent are given. In the previous work, we mainly extracted and calculated the temporal range, spatial range, AR occurrence times, AR duration and AR contribution to snowfall of the Antarctic continent. The correlation analysis of these five main calculation parameters is carried out, as shown in Fig. 8 below.

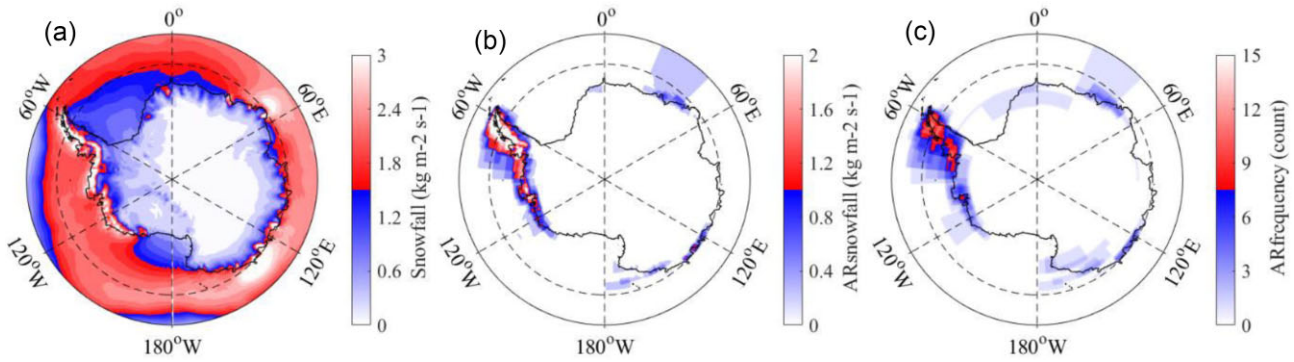

Figure 7. Total snowfall (left-hand column), AR snowfall (middle column) and AR frequency (right-hand column).

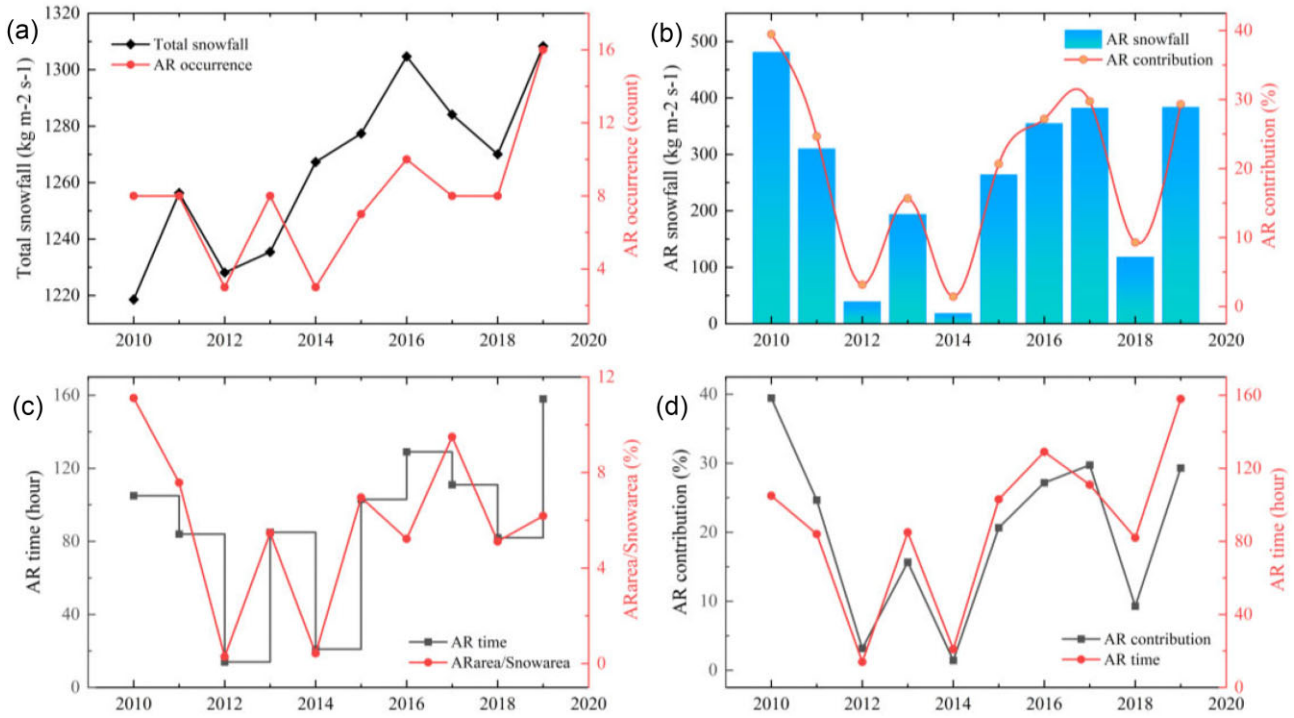

Figure 8. Correlation analysis of AR contribution.

Fig. 8(a) shows the correlation between interannual snowfall and the number of AR logins, and it can be concluded from the data that there is a positive correlation between the two; (b) shows the quantified AR snowfall and shows the contribution; (c) shows the correlation between the length of AR logins and the spatial extent of AR logins, and it can be tentatively obtained that the longer the AR stays, the greater the spatial extent of AR logins, and there is a positive correlation and (d) shows the correlation between the duration of AR logins and the contribution of AR snowfall, and it can be concluded from the linear relationship between the two that the longer the AR logins, the greater the contribution of AR snowfall, and there is a positive correlation.

By calculating the snowfall displacement for the 2010–2019 AR events (using OHI3 and DUM1 as examples), the results are shown in Fig. 9 below.

The GPS measurement stations (a)–(c) OHI3 and (d)–(f) DUM1 on the Antarctic continent are calculated in Fig. 9. When the two stations are analysed together, the snowfall displacement is relatively stable with small amplitudes in the eastward and northward directions, and relatively volatile with large vertical amplitudes. The location of the discs in Fig. 9 is the more prominent part where the vertical displacement occurs and the corresponding moment of time. This is consistent with the trend of snow displacement in 2010 in Fig. 4. In addition, the plane and vertical displacements

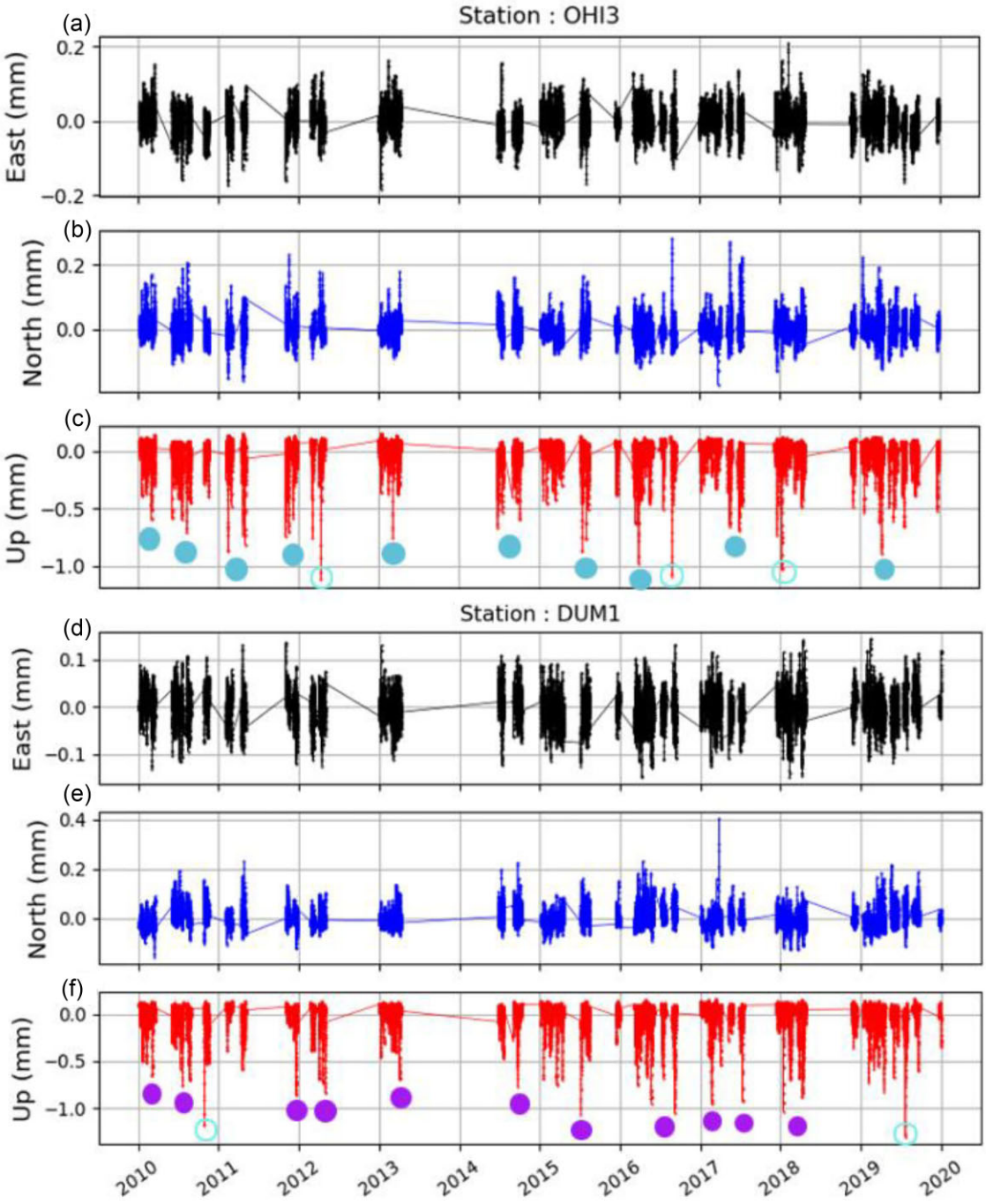

Figure 9. AR snowfall displacement calculation for the past 10 yr.

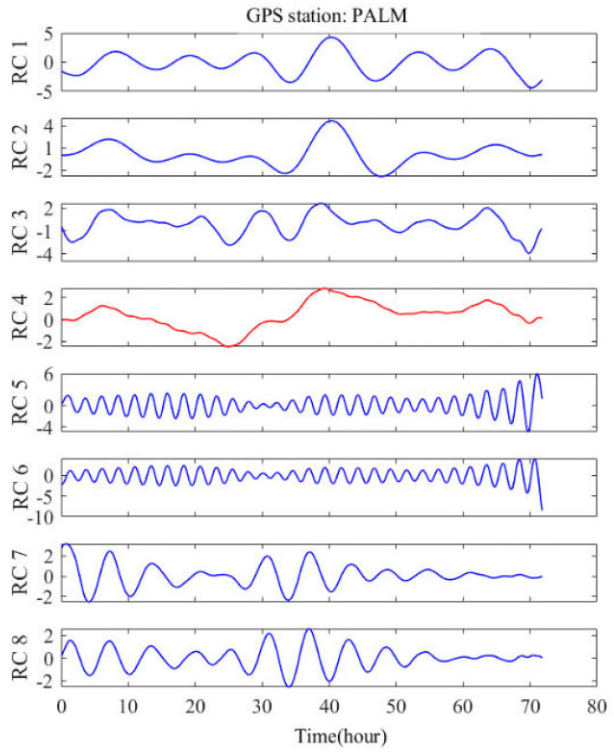

Figure 10. SSA decomposition of GPS time-series.

obtained by calculating the cumulative multiyear AR snowfall values are greater than that of 2010. From this phenomenon, it can be tentatively assumed that AR snowfall has some influence on the occurrence of displacement in the Antarctic continent, and the correlation is roughly presumed to be positive from this study.

3.4 Extraction of AR signals using SSA

The crustal deformation signal due to AR is relatively small in magnitude due to its short duration. Therefore, we extracted the AR deformation signal based on the SSA (singular spectrum analysis) method using the GNSS 5-min time-series provided by NGL. SSA can be used to process nonlinear time-series data, decompose the original time-series into a series of signal components, construct a trajectory matrix, decompose and reconstruct the time-series, and each component can be classified into periodic, quasi-periodic, noise and trend components. It has been widely used in GNSS time-series analysis (Hassani 2007; Kong *et al.* 2023; Yu *et al.* 2021). We used GNSS with AR snowfall displacement time-series to form SSA with a total time-series length of 862 and a window setting of 180, and the extraction results are shown in Fig. 10 below.

In Fig. 10, RC1–RC8 are the eight component signals reconstructed by GNSS using SSA, excluding the common annual weekly signal, semi-annual weekly signal and the interference of noise signal, and initially locking the AR displacement signal to RC4. Similarly, SSA analysis is performed on other stations to verify the AR signal, and deformation contribution analysis is summarized in Fig. 11.

In Fig. 11, the black curve represents the extracted AR displacement component signal from GNSS, the red curve represents the AR snowfall displacement component signal and the blue curve represents the GNSS-AR fitted displacement signal, this is for the AR-induced GNSS displacement component, which is a simulated curve close to the theoretical values which is mainly used to locate the moment of sudden signal change due to AR. According to the results presented by the three curves, the AR snowfall displacement and GNSS-AR displacement components are analysed in conjunction with the period of AR appearance. It can be seen from Fig. 11 that the GNSS station time-series amplitudes all increase significantly at the moment of AR appearance. the crustal deformation displacement due to AR is in good agreement with the signal extracted by GNSS, considering that snowfall is a continuous accumulation process, so there is a slight lag in GNSS displacement relative to AR. The statistics found that the maximum AR snowfall load deformation variable was about 1.63 mm, and the extracted GNSS-AR displacement signals were generally concentrated at about 3 mm. Further study found that the GNSS and AR snowfall load deformation displacements at stations OHI3, PALM, VESL, ROTHand DUPT showed an increasing trend and peaked during the AR occurrence period. In addition, we take into account the lag of AR login impact by extending the AR login start and end times by about 24 hr each before and after the determination of the AR login. As in Fig. 11, the GPS sites LPLY and MAW1, the load-deformation did not peak during the occurrence of AR, but showed a continuously increasing trend and peaked about 10 hr after the end of AR.

4 DISCUSSION

In our preliminary work, we focused on quantifying the AR snowfall of the Antarctic continent, so we first designed a spatial constant matrix method, which mainly extracted and calculated the time range, spatial range, AR login times, AR login duration and AR contribution to snowfall of the Antarctic continent. The correlation analysis was performed for these five main calculated parameters, as shown in Fig. 8(a) shows the correlation between interannual snowfall and the number of AR logins, and it can be concluded from the data that there is a positive correlation between the two; (b) shows the quantified AR snowfall and shows the contribution; (c) shows the correlation between the length of AR logins and the spatial extent of AR logins, and it can be tentatively obtained that the longer the AR stays, the greater the spatial extent of AR logins, and there is a positive and (d) shows the correlation between the length of AR logins and the contribution of AR snowfall, and it can be concluded from the linear relationship between the two that the longer the AR logins, the greater the contribution of AR snowfall, and there is a positive correlation. Then the snowfall is calculated for the local location where the AR is located, and the snowfall due to the AR is separated from the interannual snowfall. The research results of AR in 2010–2019 show that the number of AR logins directly affects the total duration of AR stay in the Antarctic continent. The longer the total duration of AR logins in a year, the more snowfall will increase. So, AR plays an important role in snowfall contribution to the Antarctic continent, and the maximum interannual contribution reaches 29.78 per cent. From the visual processing in Figs 6(b), (e) and (h) and in Fig. 7(b), it can be concluded that the contribution of AR to snowfall is more prominent in the West Antarctic, especially in the Antarctic Peninsula. From 2010 to 2019, the AR logged into the Antarctic Peninsula every year, significantly increasing the snowfall in the Antarctic Peninsula. Finally, the snowfall located in each plate of the Antarctic continent regarding the time of AR appearance and coverage is quantified and calculated. When the quantitative calculation of AR snowfall is completed, we correlate the calculated results. In the later work,

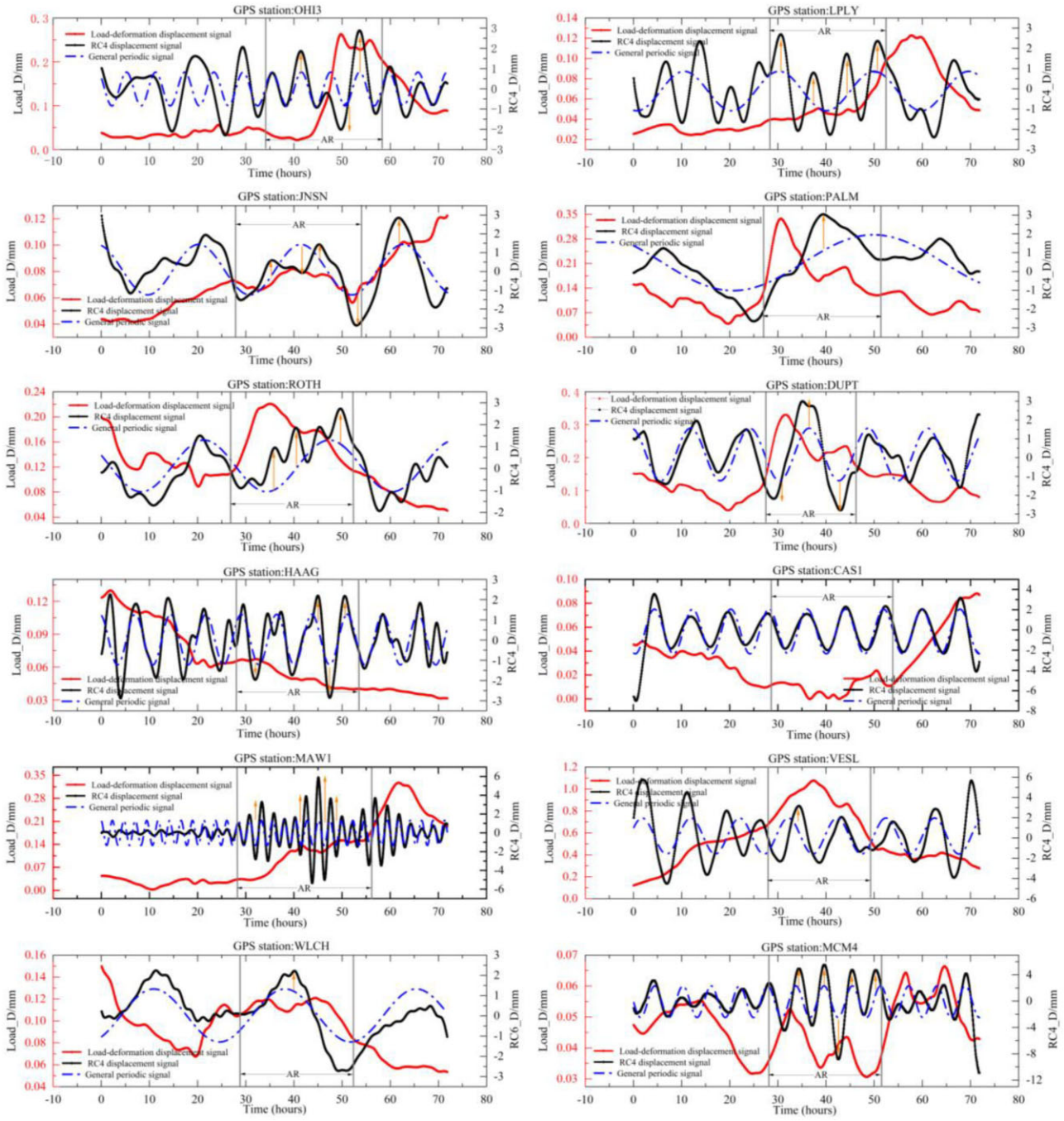

Figure 11. Verification of AR displacement signal and deformation contribution.

we mainly analyse the AR snowfall and displacement calculations to study the influence of AR snowfall on the displacement of the Antarctic continent, to quantify and analyse the contribution of snowfall to displacement, and to derive the relationship between AR snowfall and displacement, and we hope that the results of the study will provide some favourable references to the Antarctic environment and Antarctic-related research. In particular, it is a basic theoretical support for our upcoming next research.

AR snowfall causes displacement changes. In this study, the load-deformation model is used for the calculation of displacements. The results of the calculations for a single- and multiyear accumulation show that AR snowfall has a greater effect on vertical displacement than plane displacement. The displacement calculation is continued for 34 GPS reference stations spread across the Antarctic continent, and the various characteristics of the displacement by distance from the coastline position are analysed. The results from the study of several regions of the Antarctic continent (East Antarctica, Amundsen Sea, Ross Ice Shelf, Ronne Ice Shelf, SAP and NAP) show that the average and maximum displacements tend to be maximum at points closer to the coastline, and vice versa, smaller. The AR is transported from low latitude to high latitude, and the AR enters the Antarctic continent firstly by contacting the coastline, and the AR will not extend to the interior of the Antarctic continent in large quantities, so the AR is mainly concentrated near the coastline.

On two points of speculation. First, it is worth noting that during the extraction of AR information, we found that the AR does not enter the Antarctic continent extensively and rarely continues to extend to the centre of the Antarctic continent, and the AR changes its shape from bar-like to elongated or filamentary when it approaches or is about to enter the Antarctic continent. In addition, we also found that many times the AR suddenly leaves the Antarctic continent when it is about to land and returns to a broader strip when it leaves. We speculate whether there is a special force balancing the AR login in the Antarctic continent. Our existing results show that the AR contributes to a high degree of snowfall in the Antarctic continent, and if a large number of ARs are login in the Antarctic continent, it may cause a sharp increase in snowfall, followed by large displacement or more extreme weather, and may also cause a disruption of the mass balance between the Antarctic continent and the ice surface. Second, speculation on the stability of the Antarctic Peninsula ice shelf. In the study of this paper, AR was found to be logged in the Antarctic Peninsula in several iterations during 2010–2019, as shown in Fig. 7(b). According to Wille *et al.* (2022), a strong AR can weaken the stability of the ice shelf. Therefore, from the results of the present study on the frequent and intensive coverage of the Antarctic Peninsula by AR, combined with the recent findings of Wille *et al.* (2022), it can be inferred that the stability of the Antarctic Peninsula ice shelf is being continuously weakened by AR events.

5 CONCLUSION

AR is an important reference factor for studying snowfall in the Antarctic continent, and the following conclusions are drawn from the research and analysis of snow contribution and displacement contribution.

(1) The contribution of AR to snowfall in the Antarctic continent was quantified by extracting the spatial and temporal extent of AR and processing the spatial matrix of snowfall. the contribution of AR to snowfall in 2010–2019 was 39.45, 24.65, 3.16, 15.66, 1.42, 20.66, 27.17, 29.73, 9.28 and 29.30 per cent. the contribution was smaller in 2012 and 2014, and there was a gradual increase in the contribution in 2010, 2015, 2016, 2017 and 2019, and the impact of AR on snowfall in the Antarctic continent mainly ranged from 9.28 to 29.73 per cent.

(2) After visualizing the distribution of AR snowfall in the Antarctic continent, AR snowfall mainly occurs in Antarctic Peninsula and Marie Byrd Land located in West Antarctica, Adélie Land, Wilkes Land and Enderby Land in East Antarctica, and the above areas dominate the entire Antarctic continent. According to the calculation of snow load displacement in the Antarctic continent, the vertical displacement at the onset of AR is significantly larger than at the onset of non-AR. According to the data characteristics and phenomena in this paper, it can be determined that AR snowfall has a more significant impact on the occurrence of Antarctic continent displacement, and it can be inferred from this paper that the relationship between the two is a positive correlation.

(3) Considering the effect of location from the coastline on deformation, the results show that the closer the coastline is, the closer the average and maximum displacement of the points tend to be to the maximum, and vice versa, the smaller. It further illustrates the significant effect of AR on snowfall displacement and the characteristics of displacement variation.

AUTHOR CONTRIBUTIONS

Conceptualization, W.L.; methodology, J.L. and W.L.; software, J.L., validation, C.K.S. and W.L.; formal analysis, J.L.; investigation, S.Z.; resources, W.L.; data curation, W.L.; writing original draft preparation, J.L. and W.L.; writing review and editing, J.L. and C.K.S.; visualization, J.L.; supervision, C.K.S.; project administration, F.L. and J.T.L.; funding acquisition, F.L. All authors have read and agreed to the published version of the manuscript

DATA AVAILABILITY

The MERRA-2 snowfall data used in this study are available at: https://disc.gsfc.nasa.gov/datasets/M2T1NXLFO_5.12.4/summary?keywords=snowfall; the GPS time-series used in this study are available at:http://geodesy.unr.edu/NGLStationPages/GlobalStationList; the original Load-deformation model and procedure description documents (PDF) used in this study is available at: https://github.com/hrmartens/LoadDef and the location information of the Antarctic GPS stations are available at:https://www.unavco.org/data/gps-gnss/gps-gnss.html.

FUNDING

This research was funded by the National Natural Science Foundation of China (42 074 006), the National Key Research and Development Program of China (2017YFA0603104) and The State Key Program of the National Natural Science Foundation of China (41 531 069).

REFERENCES

Adusumilli, S., Fish, A., Fricker, H.A. & Medley, B. 2021. Atmospheric river precipitation contributed to rapid increases in surface height of the west Antarctic ice sheet in 2019. *Geophys. Res. Lett.,* **48**(5), e2020GL091076.

Bevis, M. *et al.* 2009. Geodetic measurements of vertical crustal velocity in West Antarctica and the implications for ice mass balance. *Geochem. Geophys. Geosyst.,* **10**(10).

Collow, A., Shields, C.A., Ramos, A.M. & Guan, B. 2022. Atmos pheric rivers: processes, impacts, and uncertainty quantification. Part I, in *102nd American Meteorological Society Annual Meeting*. AMS, https://ams.confex.com/ams/102ANNUAL/meetingapp.cgi/Session/58943.

Djoumna, G. & Holland, D.M. 2021. Atmospheric rivers, warm air intrusions, and surface radiation balance in the Amundsen Sea Embayment. *J. geophys. Res.,* **126**(13), e2020JD034119.

Francis, D., Mattingly, K.S., Temimi, M., Massom, R. & Heil, P. 2020. On the crucial role of atmospheric rivers in the two major Weddell Polynya events in 1973 and 2017 in Antarctica. *Sci. Adv.,* **6**(46), eabc2695.

Gimeno, L., Algarra, I., Eiras-Barca, J., Ramos, A.M. & Nieto, R. 2021. Atmospheric river, a term encompassing different meteorological patterns. *WIREs Water,* **8**(6), e1558.

Gorodetskaya, I.V., Tsukernik, M., Claes, K., Ralph, M.F., Neff, W.D. & Van Lipzig, N.P. 2014. The role of atmospheric rivers in anomalous snow accumulation in East Antarctica. *Geophys. Res. Lett.,* **41**(17), 6199–6206.

Hassani, H., 2007. Singular spectrum analysis: methodology and comparison. *Data Sci. J.*, **5**(2007), 239–257.

Kong, Q., Zhang, L., Han, J., Li, C., Fang, W. & Wang, T. 2023. Analysis of coordinate time series of DORIS stations on Eurasian plate and the plate motion based on SSA and FFT. *Geod. Geodynam.,* **14**(1), 90–97.

Lavers, D.A. & Villarini, G. 2013. The nexus between atmospheric rivers and extreme precipitation across Europe. *Geophys. Res. Lett.,* **40**(12), 3259–3264.

Lenaerts, J.T., Medley, B., van den Broeke, M.R. & Wouters, B. 2019. Observing and modeling ice sheet surface mass balance. *Rev. Geophys.,* **57**(2), 376–420.

Maclennan, M.L. *et al.* 2022. Climatology and surface impacts of atmospheric rivers on West Antarctica. *Cryos. Discus.,* 1–25, https://doi.org/10.5194/tc-17-865-2023.

Maclennan, M.L. & Lenaerts, J.T. 2021. Large-scale atmospheric drivers of snowfall over Thwaites Glacier, Antarctica. *Geophys. Res. Lett.,* **48**(17), e2021GL093644.

Martens, H.R., Rivera, L. & Simons, M. 2019. LoadDef: a Python-based toolkit to model elastic deformation caused by surface mass loading on spherically symmetric bodies. *Earth Space Sci.,* **6**(2), 311–323.

Mattingly, K.S. *et al.* 2020. Strong summer atmospheric rivers trigger Greenland Ice Sheet melt through spatially varying surface energy balance and cloud regimes. *J. Clim.,* **33**(16), 6809–6832.

Nash, D., Waliser, D., Guan, B., Ye, H. & Ralph, F.M. 2018. The role of atmospheric rivers in extratropical and polar hydroclimate. *J. geophys. Res.,* **123**(13), 6804–6821.

Neiman, P.J., Hughes, M., Moore, B.J., Ralph, F.M. & Sukovich, E.M. 2013. Sierra barrier jets, atmospheric rivers, and precipitation characteristics in Northern California: a composite perspective based on a network of wind profilers. *Mon. Weather Rev.,* **141**(12), 4211–4233.

Neiman, P.J., Ralph, F.M., Wick, G.A., Lundquist, J.D. & Dettinger, M.D. 2008. Meteorological characteristics and overland precipitation impacts of atmospheric rivers affecting the West Coast of North America based on eight years of SSM/I satellite observations. *J. Hydrometeorol.,* **9**(1), 22–47.

Pawlowicz, R. 2020. M_Map: a mapping package for MATLAB, version 1.4 m. *Computer Software,* UBC EOAS.

Payne, A.E. *et al.* 2020. Responses and impacts of atmospheric rivers to climate change. *Nat. Rev. Gastroenterol. Hepatol.,* **1**(3), 143–157.

Pohl, B. *et al.* 2021. Relationship between weather regimes and atmospheric rivers in East Antarctica. *J. geophys. Res.,* **126**(24), e2021JD035294.

Ralph, F.M. *et al.* 2017. Atmospheric rivers emerge as a global science and applications focus. *Bull. Am. Meteorol. Soc.,* **98**(9), 1969–1973.

Scott, R.C., Nicolas, J.P., Bromwich, D.H., Norris, J.R. & Lubin, D. 2019. Meteorological drivers and large-scale climate forcing of West Antarctic surface melt. *J. Clim.,* **32**(3), 665–684.

Shields, C.A. & Kiehl, J.T. 2016. Simulating the pineapple express in the half degree community climate system model, CCSM4. *Geophys. Res. Lett.,* **43**(14), 7767–7773.

Shields, C.A., Wille, J.D., Marquardt Collow, A.B., Maclennan, M. & Gorodetskaya, I.V. 2022. Evaluating uncertainty and modes of variability for antarctic atmospheric rivers. *Geophys. Res. Lett.,* **49**(16), e2022GL099577.

Terpstra, A., Gorodetskaya, I.V. & Sodemann, H. 2021. Linking sub-tropical evaporation and extreme precipitation over East Antarctica: an atmospheric river case study. *J. geophys. Res.,* **126**(9), e2020JD033617.

Turner, J. *et al.* 2019. The dominant role of extreme precipitation events in Antarctic snowfall variability. *Geophys. Res. Lett*., **46**(6), 3502–3511.

Viceto, C., Gorodetskaya, I.V., Rinke, A., Maturilli, M., Rocha, A. & Crewell, S. 2022. Atmospheric rivers and associated precipitation patterns during the ACLOUD and PASCAL campaigns near Svalbard (May–June 2017): case studies using observations, reanalyses, and a regional climate model. *Atmos. Chem. Phys.,* **22**(1), 441–463.

Wille, J.D., Favier, V., Dufour, A., Gorodetskaya, I.V., Turner, J., Agosta, C. & Codron, F. 2019. West Antarctic surface melt triggered by atmospheric rivers. *Nat. Geosci.,* **12**(11), 911–916.

Wille, J.D. *et al.* 2021. Antarctic atmospheric river climatology and precipitation impacts. *J. geophys. Res.,* **126**(8), e2020JD033788.

Wille, J.D. *et al.* 2022. Intense atmospheric rivers can weaken ice shelf stability at the Antarctic Peninsula. *Commun. Earth Environ.,* **3**(1), 90.

Yu, H., Sośnica, K. & Shen, Y. 2021. Separation of geophysical signals in the LAGEOS geocentre motion based on singular spectrum analysis. *Geophys. J. Int.,* **225**(3), 1755–1770.

Zhu, Y. & Newell, R.E. 1994. Atmospheric rivers and bombs. *Geophys. Res. Lett.,* **21**(18), 1999–2002.